

METALLICITY-CORRECTED TIP OF THE RED GIANT BRANCH DISTANCE TO NGC 4258

Violet A. Mager, Barry F. Madore & Wendy L. Freedman

The Observatories
Carnegie Institution of Washington
813 Santa Barbara St.
Pasadena, CA 91101

Draft version June 21, 2024

ABSTRACT

We have determined the distance to NGC 4258 using observations made with the Hubble Space Telescope (HST) and the Wide Field, Advanced Camera for Surveys (ACS/WFC). We apply a modified technique that fully accounts for metallicity effects on the use of the luminosity of the tip of the red giant branch (TRGB) to determine one of the most precise TRGB distance moduli to date: $\mu(\text{TRGB}) = 29.28 \pm 0.04$ (random) ± 0.12 (systematic) mag. We discuss this distance modulus with respect to other recent applications of the TRGB method to NGC 4258, and with several other techniques (Cepheids and masers) that are equally competitive in their precision, but different in their systematics.

Subject headings: distance scale – galaxies: individual (NGC 4258)

1. INTRODUCTION

This is the first in a short series of papers using a refined methodology for determining distances using the discontinuity in the I-band magnitude of the red giant branch luminosity function as a standard candle (Lee et al. 1993), the so-called TRGB (tip of the red giant branch) method. Here we apply a new methodology in correcting for the now well understood and precisely calibrated metallicity effects on the TRGB magnitude (see Section 4.1 and Madore et al. 2008).

Our first target is the spiral galaxy NGC 4258. It is nearby, and therefore very highly resolved, not only into its bright, high-mass Population I disk stars, but also into its fainter, but still accessible, low-mass Population II halo stars. NGC 4258 contains many known Cepheids that have been discovered and used as distance indicators in multiple observing campaigns using HST. Its halo has been resolved and studied on equally as many occasions, revealing a broad, richly populated giant branch for TRGB distance determination. The uniqueness of NGC 4258 lies at its center, where a Keplerian-rotating disk of water masers has proper motions and radial velocities that can be cross-compared and modeled with essentially one additional free parameter: the distance. As such, the independently calibrated Population I (Cepheid) and Population II (TRGB) distance scales both converge on and cross at NGC 4258, where they can be compared to that from simple geometry (maser method). No other galaxy provides such an environment for testing the distance scale. That said, it must also be emphasized that NGC 4258 is still only one object, and its uniqueness means that there is no independent check on the maser distance methodology itself, its random errors, or its systematics.

Without prejudice as to which (if any) of the three distance determination methods discussed here is better (understood or calibrated) at this point, we now proceed to present a new and improved determination of the TRGB distance using HST ACS/WFC data from one

of our approved and scheduled programs, and archival WFPC2 data as a consistency check. We compare these results with previous TRGB results, and with the other past and published methods.

2. DATA REDUCTION AND CALIBRATION OF THE ACS IMAGES

Our HST/ACS observations of the NGC 4258 halo (PID 9477, PI Madore, B.F.) consist of 2×2850 s exposures in F555W, and 2×1300 s exposures in F814W. Figure 1 shows the location of the fields-of-view of the ACS (thick-lined polygon) and partially over-lapping archival WFPC2 (thin-lined polygons) observations, overlaid on a DSS¹ image of NGC 4258. As a consistency check, we used two different methods of identifying the stars and calibrating the photometry. Both produced TRGB magnitudes that agree to within the uncertainties. The details of each method are described below.

For the first method, we identified stars and calibrated the ACS images using the ACS module for the highly automated DOLPHOT package² (see the DOLPHOT User's Guide for details.³) We applied the DOLPHOT package to the STSCI pipeline-processed and cosmic-ray cleaned images of NGC 4258, masking bad pixels and using the recommended settings given in the DOLPHOT/ACS User's Guide⁴. In order to additionally reject non-stellar objects and objects with highly uncertain photometry, we selected only those detections with a DOLPHOT output type of 1 (determined by DOLPHOT to be a "good star"), with a flag of 0 (the star was "recovered well" in the image), with sharpness measure-

¹ The Digitized Sky Surveys were produced at the Space Telescope Science Institute under U.S. Government grant NAG W-2166. The images of these surveys are based on photographic data obtained using the Oschin Schmidt Telescope on Palomar Mountain and the UK Schmidt Telescope. The plates were processed into the present compressed digital form with the permission of these institutions.

² By Andrew Dolphin, <http://purcell.as.arizona.edu/dolphot/>

³ <http://purcell.as.arizona.edu/dolphot/dolphot.ps.gz>

⁴ <http://purcell.as.arizona.edu/dolphot/dolphotACS.ps.gz>

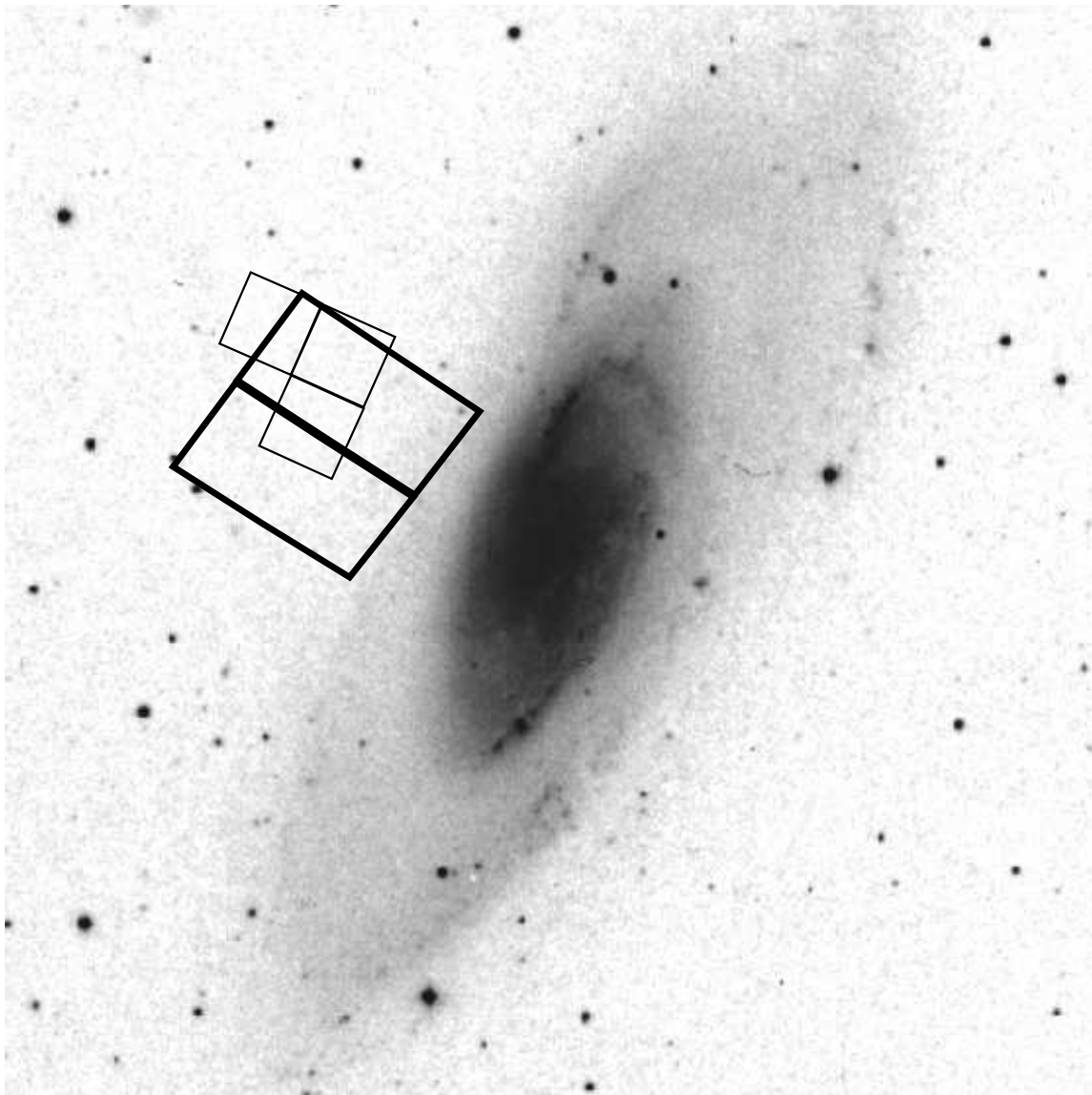


FIG. 1.— DSS image of NGC 4258 overlaid with the footprints of the HST ACS (thick-lined polygon) and WFPC2 (thin-lined polygons) images used in this analysis. North is up, and east is to the left.

ments of -0.3 to $+0.3$, and with a crowding parameter < 0.5 mag. We then applied Galactic extinction corrections using the $E(B-V)$ reddening measurements given in the NASA/IPAC Extragalactic Database (NED), and the total-to-selective absorption ratios ($A/E(B-V)$) presented in Sirianni et al. (2005).

As a consistency check on the photometry, we also used DAOPHOT II (Stetson 1987) and ALLSTAR (Stetson 1994) to independently reduce and analyze the ACS images. We located stars within 5σ of the sky in the F814W images, applying sharpness cut-offs determined through visual inspection of the results to reject bad pixels and low surface brightness galaxies, as well as roundness cut-offs to reject bad rows, columns, and highly inclined galaxies. Any remaining bad pixels were rejected when objects whose PSF-fit photometry could not be determined for both the F814W and the F555W images were eliminated from our analysis. We rejected most of the remaining non-stellar objects (cosmic rays and/or com-

pact galaxies that coincidentally had PSF's similar to the stellar PSF) by applying a cut-off limit in the ALLSTAR χ measurement (which gives an indication of how good the PSF fit was with respect to the other objects in the group it was measured in). After visual inspection of its effects on the color-magnitude diagram (CMD), we chose $\chi_V < 2$ and $\chi_I < 3$. Aperture corrections and transformations of the F555W and F814W magnitudes to Johnson V and I, respectively, were applied following the method outlined in Sirianni et al. (2005). We then applied the Galactic extinction corrections as described above.

Method 1 (DOLPHOT) and Method 2 (DAOPHOT II/ALLSTAR) both produced consistent photometry at the brightness level of the TRGB. Our edge-detection software (as described in Section 4.2) found that the I-band magnitude of the TRGB for both photometry methods agrees to within 0.04 mag, which is within the measured uncertainties. However, we note in passing

that DOLPHOT went deeper than the 5σ cut-off used in Method 2, and reported somewhat smaller photometric uncertainties at the tip. As such, we present the photometry from DOLPHOT in all subsequent figures and analysis of the ACS data.

3. DATA REDUCTION AND CALIBRATION OF THE WFPC2 IMAGES

As a comparison, we downloaded pipeline-calibrated WFPC2 images of the NGC 4258 halo (PID 9086, PI Ferguson, H.C.) from the STScI (Space Telescope Science Institute) archive (see Fig. 1 for the location of these observations). These observations include 9×1268 s (on average) exposures in F606W, and 9×1300 s exposures in F814W. We did not use the smaller field-of-view PC chip in our analysis. We registered the individual images of each of the chips in each filter with the `IMSHIFT` task in IRAF⁵, and averaged the images (with cosmic ray rejection) using `IRAF/IMCOMBINE`. As with Method 2 for the ACS data (Section 2), we used `DAOPHOT II` and `ALLSTAR` to locate stars above 2σ of the sky, and to determine their PSF-fit magnitudes.

We applied transformations and corrections as follows. The instrumental F606W and F814W magnitudes were CTE (charge transfer efficiency)-loss corrected, aperture corrected, and transformed to Johnson V and I magnitudes (respectively) using the methods outlined in Dolphin (2000), with the updated 2002 calibration constants.⁶ The WFPC2 first- and second-order color terms are much larger than those for ACS, and required five iterations of the transformation equation to converge at the 0.001 mag level for each star. We further rejected non-stellar detections by requiring that $\chi_V < 0.9$ and $\chi_I < 1$ (see Section 2). Finally, we corrected for Galactic extinction using the $E(B-V) = 0.016$ mag reddening value calculated by NED for the Galactic line of sight to NGC 4258, and transformed to $A_V = 2.68 \times E(B-V)$ and $A_I = 1.82 \times E(B-V)$.

4. MEASURING THE APPARENT MAGNITUDE OF THE TRGB

Figure 2 shows the CMD's for NGC 4258 from the WFPC2 data (left panel) and the ACS data (right panel). The error bar in the lower right corner of each panel represents the median uncertainty on the photometry of the stars within ± 0.3 mag of the location of the TRGB. The comparison of data sets is impressive. It should be mentioned, however, that the number of stars detected in WFPC2 may have been improved with less conservative signal-to-noise cuts in `DAOPHOT II`, or by using other reduction packages, such as `HSTPHOT`.

As can be seen in these figures, there is a readily apparent luminosity above which the number density of stars drops off precipitously. We identify this discontinuity with the TRGB, which is the result of the core helium flash of red giant stars occurring at about the same bolometric luminosity for stars of all ages $\gtrsim 2$ Gyr. The I-band magnitude of this discontinuity is known to be

only weakly dependent on metallicity for sufficiently low metallicities ($[Fe/H] \lesssim -0.7$ dex) (Iben & Renzini 1983; Lee et al. 1993). At higher metallicities, line-blanketing effects begin to have a more significant effect, and corrections have been suggested to take this into account (e.g., Salaris & Cassisi 1998; Bellazzini et al. 2001, 2004; however, see below and Madore et al. 2008 for the latest calibration). As such, measuring the magnitude of this number-density drop-off, which corresponds to the tip of the red giant branch, has proven to be a reliable way of finding the distance modulus of any galaxy that has resolvable stars which are part of an existing population of old red giant stars.

We now consider the uncertainty in measuring the location of the TRGB. The most important factors include random photometric errors, sample size, crowding issues, and contamination/confusion caused by asymptotic giant branch (AGB) stars (Renzini 1992; Madore & Freedman 1995). Lee et al. (1993) first introduced a quantitative method of measuring the magnitude of the TRGB and its uncertainty. They used a zero-sum (Sobel) kernel edge-detector $[-1, 0, 1]$ applied to the binned histograms of the observed luminosity functions. This filter produces a maximum response at the magnitude where the slope of the luminosity profile is largest. However, this method is sensitive to random noise spikes in the luminosity function, and will, of course, produce slightly different answers depending on the choice of bin size, the starting-point of the histogram, etc. (Madore & Freedman 1995; Sakai et al. 1996). To reduce the impact of noise spikes, Madore & Freedman used a modified version of the Lee et al. edge-detector, with a weighted Sobel filter that smoothed the data over 2 bins on either side of the central bin (i.e., $[-1, -2, 0, +2, +1]$). Sakai et al. (1996) went a step further, Gaussian-smoothing the luminosity distribution and applying an edge-detection filter to the continuous function, thereby avoiding the issues involved in the discrete binning. Méndez et al (2002) modified this method to take into account the natural power-law distribution of the luminosity function, using a logarithmic ratio in their edge-detection filter instead of the first derivative. Additionally, they employed a maximum-likelihood analysis as an alternative method of estimating the position of the TRGB, with uncertainties being derived from bootstrap re-sampling of the data. Mouchine et al. (2005) also used the maximum-likelihood analysis and bootstrap re-sampling to find TRGB distances to several galaxies, including NGC 4258. Other authors (e.g., Cioni et al. 2000; Sarajedini et al. 2002; Frayn & Gilmore 2003; McConnachie et al. 2004; Makarov et al. 2006) have additionally modified these and similar techniques, reducing the contribution of random noise spikes in the luminosity function. Madore et al. (2008) discuss yet another modification to the basic technique, this time aimed at capturing the metallicity-sensitivity of the TRGB itself. A similar methodology is described and applied below.

One problem inherent in all of these methods is that for some galaxies, the edge-detector can produce multiple peaks (some of which are larger than the one at the location of the TRGB itself). Choices were then made by eliminating peaks based on a priori knowledge of the general location of the TRGB. It is most desirable to remove this ambiguity, and develop an algorithm that can pro-

⁵ IRAF is distributed by the National Optical Astronomy Observatories, which are operated by the Association of Universities for Research in Astronomy, Inc., under cooperative agreement with the National Science Foundation.

⁶ http://purcell.as.arizona.edu/wfpc2_calib/

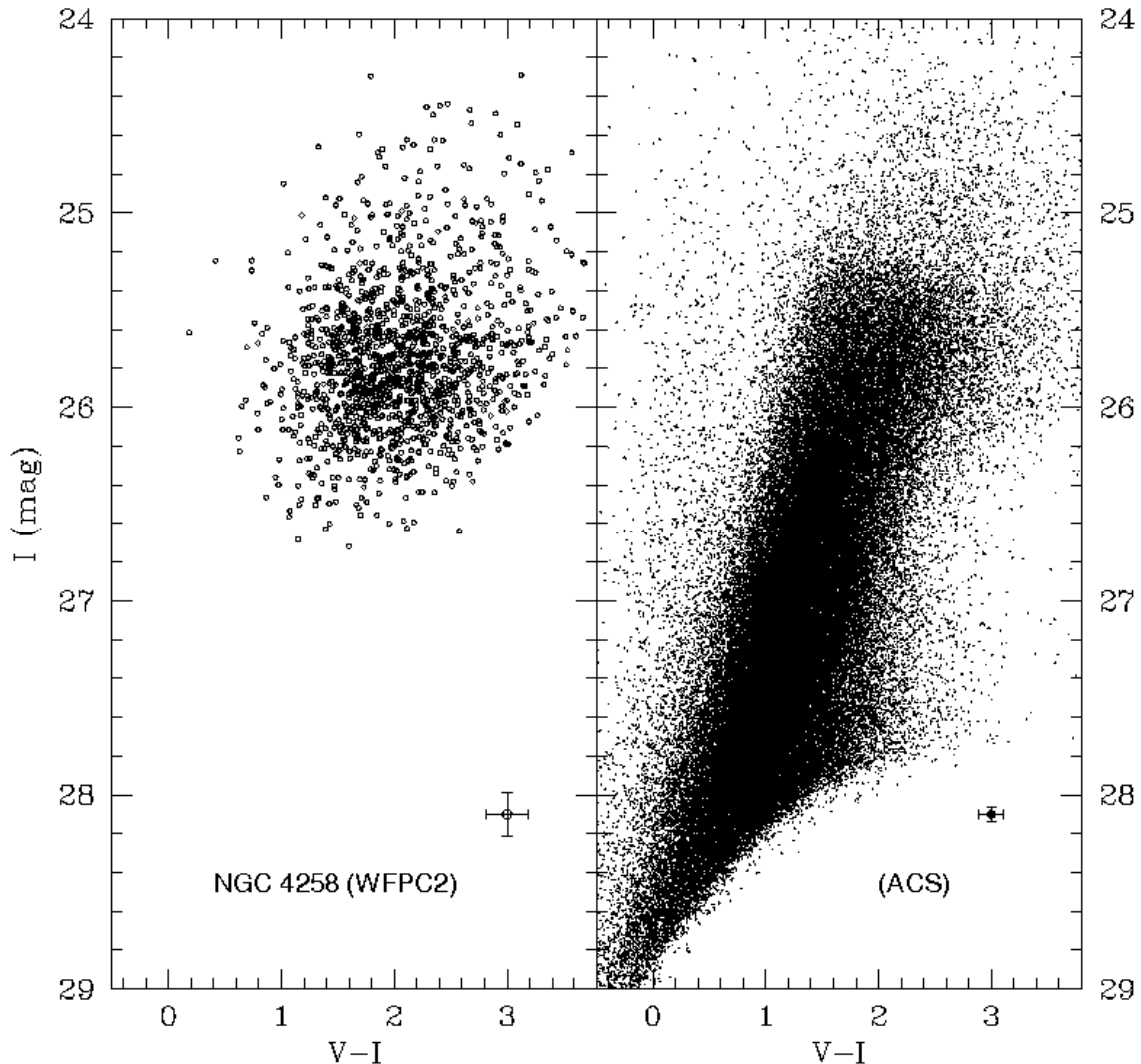


FIG. 2.— Color-magnitude diagrams for NGC 4258 from the WFPC2 data (left panel) and the ACS data (right panel). The error bar in the lower right corner of each panel represents the median uncertainty on the photometry of the stars within ± 0.3 mag of the TRGB.

duce a reliable result without added intervention. For this analysis, we employ another method of measuring the magnitude of the TRGB that is robust against random noise spikes in the luminosity profile, yet does not rely on fitting the data to any adopted model.

Uncertainties are introduced in the TRGB distance modulus by the metallicity dependence of the magnitude of the TRGB (Bellazzini 2001). This can be seen as a color dependence of the TRGB magnitude that is apparent in the ACS CMD in Fig. 2 (right panel): the edge associated with the TRGB is sloped slightly downward, becoming fainter at redder colors. Past studies have dealt with this issue by fitting a Gaussian to the color distribution of the TRGB stars, and using the peak of this distribution to determine the average metallicity of the stars, which in turn was used to correct the tip magnitude to a fiducial metallicity/color. We side-step this process by applying a metallicity correction to each star before running the edge-detection software.

In the following sections we discuss our modified version of a metallicity-corrected Sobel edge-detector, and use it to determine our TRGB distance to NGC 4258.

4.1. Correcting for Metallicity Dependence

Bellazzini et al. (2001, 2004) re-affirmed that both the absolute magnitude (M_I^{TRGB}) and color of a star at the tip of the red giant branch are functions of metallicity as given by the following relations:

$$M_I^{TRGB} = 0.14[Fe/H]^2 + 0.48[Fe/H] - 3.629 \quad (1)$$

$$(V - I) = 0.581[Fe/H]^2 + 2.472[Fe/H] + 4.013 \quad (2)$$

Clearly, these equations can be solved simultaneously to obtain M_I^{TRGB} as a function of the tip ($V-I$) color. We have numerically solved these simultaneous equations for the run of absolute magnitude with color. Those data points are shown in Fig. 3; the relation is clearly non-linear, but two rough linear approximations are shown

(note that there is a secondary solution to the resulting quadratic equation that has been rejected here as it does not fit the data or theory well). The dashed line has a slope of 0.20, and is a very good approximation to the plotted points red-ward of $(V-I) = 2.0$ mag, but it systematically deviates to brighter magnitudes by up to 0.1 mag at $(V-I) = 1.6$ mag. However, it approximates the theoretical points over the entire color range of interest with a residual scatter of only ± 0.026 mag. This slope also has observational support from Rizzi et al. (2007). The solid line shows a linear solution of slope 0.15 over the entire TRGB color range seen in nature, but it does not fit the theoretical data points as well. The linear approximation with slope $= 0.20 \pm 0.05$ is used in Madore et al. (2008), as it agrees within the error with both the observationally determined TRGB slope, and the linear fit to the analytical solution (pictured by the circled points in Fig. 3). For accuracy, we apply the full analytical solution to the data for this paper, although the linear approximation (like that given in Madore et al. (2008)) is a valid alternative.

Armed with an equation describing the magnitude of the TRGB with color we can now correct the magnitudes of all stars for metallicity before running the tip detection algorithm down through the color-magnitude diagram. With this correction applied, we find consistent results in the ACS data with color for the I-band apparent magnitude of the TRGB (I_{TRGB}) in sub-samples of stars over the range $1.6 \lesssim (V-I) \lesssim 3.0$ (see Section 4.2 for an explanation of how I_{TRGB} is measured). As such, we have effectively removed the metallicity dependence of the I_{TRGB} measurement and implicitly normalized the resulting I-band magnitudes to that of a TRGB star with $(V-I) = 1.60$ mag. This corresponds to $[Fe/H] = -1.52$, and $M_I^{TRGB} = -4.04 \pm 0.12$ mag (with the uncertainty on M_I^{TRGB} determined by Bellazzini et al. 2001, 2004). As can be seen in the left panel of Fig. 5, this transformation (by construction) removes the downward slope of the TRGB edge that is clearly seen in the right panel of Fig. 2.

This process offers an improvement over previous methods of using the average color of the TRGB stars to determine the average value of M_I^{TRGB} . It also eliminates the need to apply a red color cut-off to the TRGB, which has previously been done to avoid the region where the TRGB magnitude is increasingly depressed by metallicity and/or contaminated by extended AGB stars. This increases the fraction of stars usable in the edge-detector, and thus decreases the uncertainty of the result through higher number statistics.

4.2. Weighted Edge-Detector and Results from the ACS data

As in Méndez et al. (2002), we accommodate the power-law distribution of the luminosity profile by utilizing a logarithmic ratio in our edge detector. For the purpose of eliminating the necessity to fit the data to theoretical models, however, we apply this directly to the histogram of the I-band luminosity distribution, and test the results as a function of bin-size. We also normalize the edge-detector output by the Poisson noise, expected from \sqrt{N} statistics. The basic form of the edge-detector

yields an output filter response at the i th magnitude bin of:

$$\eta_i^o = \sqrt{N} \times (\log(m_{i+1}) - \log(m_{i-1})), \quad (3)$$

where N is the number of stars in the central i th magnitude bin. The magnitude bin corresponding to the maximum peak of η_i^o gives the magnitude at which the change in luminosity from one bin to the next is the largest. We identify that maximum response with the TRGB.

We tested this basic edge-detector by applying it to the luminosity histogram of the metallicity-corrected NGC 4258 ACS data. To eliminate contamination from non-RGB stars, we included only stars with colors corresponding to those of the TRGB, and for which the measured value of I_{TRGB} from the weighted edge detector (as given by Eq. 5) is consistent with sub-selections in color ($1.6 < (V-I) < 3.0$). The I-band histogram of these data is presented in Fig. 4 (a), using a bin size of 0.02 mag. Fig. 4 (b) shows the basic edge detector response (η^o from Eq. 4) to this histogram. At this resolution the detector response is noisy, with multiple peaks having comparable significance. The maximum peak is at $I = 25.20$ mag, but it is unconvincing. This is the case even though we have exquisite number statistics, with over 10,000 stars in the 1 mag bin below the TRGB. Past studies with shallower data have typically had number statistics close to or below the statistical limit at which the TRGB method was considered to be reasonably accurate (i.e., 50 – 100 stars in the single magnitude bin below the TRGB, Madore & Freedman 1995). Problematic to these past studies, a recent analysis has found an even stricter statistical limit of 400-500 stars (Madore et al. 2008). The filter response is even more noisy for data with lower number statistics, in which case taking different sub-samples of stars or even slightly changing the starting magnitude and bin size can cause one of the other peaks to be randomly higher. In some cases it can yield a vastly different answer for the magnitude of the steepest edge. For instance, we see this effect in our data if we choose a smaller sub-sample of stars by making a color cut of $1.6 < (V-I) < 2.0$. There are still more than enough stars to meet the minimum requirement for this method (i.e., 5,900 stars in the mag bin below the TRGB), but the highest peak in the edge detector response is now at 26.36 mag, which corresponds to the second highest peak, previously seen in Fig. 4(b). This is a typical problem with Sobel detectors (even those that fit the data to a smooth curve), and has been alleviated by some in the past by picking the peak that corresponds to the most likely location of the TRGB as seen in the CMD. It is desirable to remove this ambiguity by modifying the edge detector so that a priori assumptions about the general location of the magnitude of the TRGB are unnecessary, even in data-sets with lower number statistics.

If we use wider bins, we effectively smooth the data and thereby reduce the noise, at the cost of precision of our result and potentially washing out important structures within the luminosity profile. We now explore this option. Using bins of size 0.05 mag still leaves ambiguous spikes, as seen when using the 0.02 mag bins. These ambiguous cases begin to disappear when we use bins 0.10 mag in size. As shown in Fig. 4(c), there is now

TRGB Theory (Bellazzini 2001, 2004)

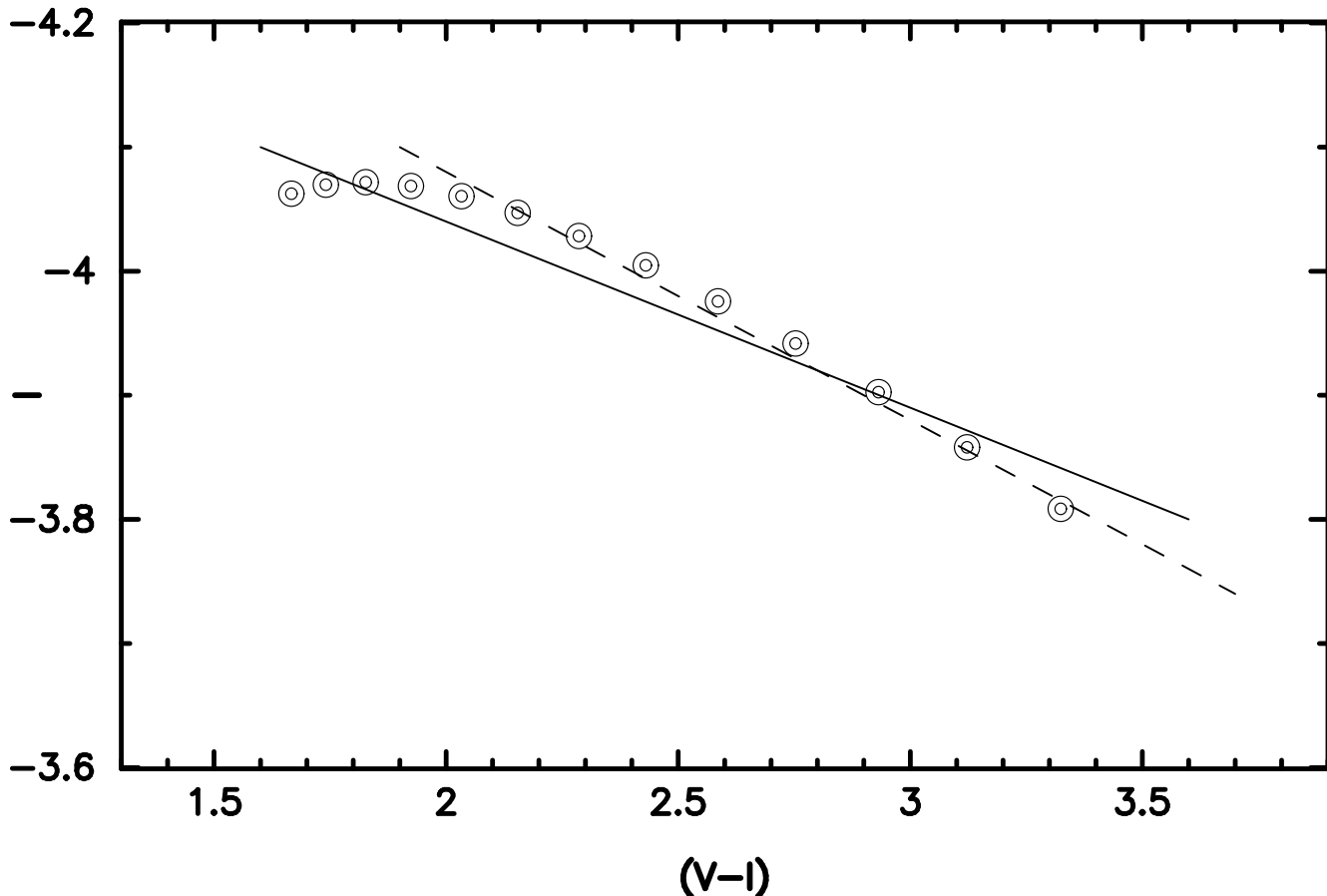


FIG. 3.— The theoretical dependence of the absolute I-band magnitude of a TRGB star on its $(V-I)$ color, as derived from the relations of M_I^{TRGB} and $(V-I)$ vs. metallicity (Bellazzini et al. 2001, 2004). The solid line shows a rough fit over the color range $(V-I) \sim 1.6-3.6$, with a drop of 0.15 mag/mag. The dotted line has a slope of 0.20 mag/mag which is a closer fit to theory for colors redder than ~ 2.0 , and which is more closely supported by the observations of Rizzi et al. (2007). One is left with the following choices: (a) a linear approximation of shallow (0.15) slope representing the (non-linear) trend over the entire color range seen for TRGB stars, (b) a steeper linear approximation of slope 0.15 which more closely approximates the theory (and the restricted observations), but only over a more narrowly-defined and redder range of color than observed, or (c) applying the detailed non-linear theoretical correction to the data over the full color range. Striving for accuracy, we use method c, removing this color dependence in our analysis and arbitrarily normalizing the TRGB stars to the I-band magnitude of a TRGB star with a color of $(V-I) = 1.6$.

only one statistically significant peak at ~ 25.30 mag, which is roughly near the by-eye location of the TRGB in the CMD in Fig. 5. Unlike the 0.02 bin-size edge detector, this result is robust when testing it on smaller sub-samples of stars. Using bins much larger than 0.10 mag over-smoothes the data, and the TRGB edge becomes undetectable.

We can achieve the best of both worlds by convolving the high precision 0.02 mag bin-size filter (which has high precision but is sensitive to noise) with the 0.10 mag bin-size filter (which is over-smoothing the data, but is robust to high-frequency noise-spikes in the luminosity profile). We do this for a histogram with original bin widths of 0.02 mag, by modifying Eq. 4, such that we take the logarithmic ratio of the sum of the 5 bins fainter and 5 bins brighter than the i th magnitude bin. We then step the filter by 0.02 mag in turn, producing a filter response, η , for every 0.02 mag in the histogram. We again normalize this output by the Poisson noise in

the central three bins in order to properly reduce significance of the noise-induced fluctuations in the filter response. The new modified equation for the weighted edge-detector response at the i th magnitude bin is:

$$\eta_i = \sqrt{\sum_{i-1}^{i+1} N_n} \times \left(\log\left(\sum_{i+1}^{i+5} m_n\right) - \log\left(\sum_{i-5}^{i-1} m_n\right) \right). \quad (4)$$

Fig. 5 displays the results of applying this weighted edge-detection filter to the NGC 4258 ACS data. The left panel of Fig. 5 shows the CMD with the metallicity correction derived from Eq.'s 2 and 3 applied to each star. The right panel shows the edge-detector filter response, η , from Eq. 5. The shape of this response is a combination of the large-scale response from the 0.10 mag bin basic filter from Eq. 4 (see Fig. 4 (c)), and the higher precision, small-scale filter response of the 0.02 mag bin basic filter (Fig. 4 (b)). The result is an unambiguous maximum peak at $I = 25.24$ mag, which is marked on

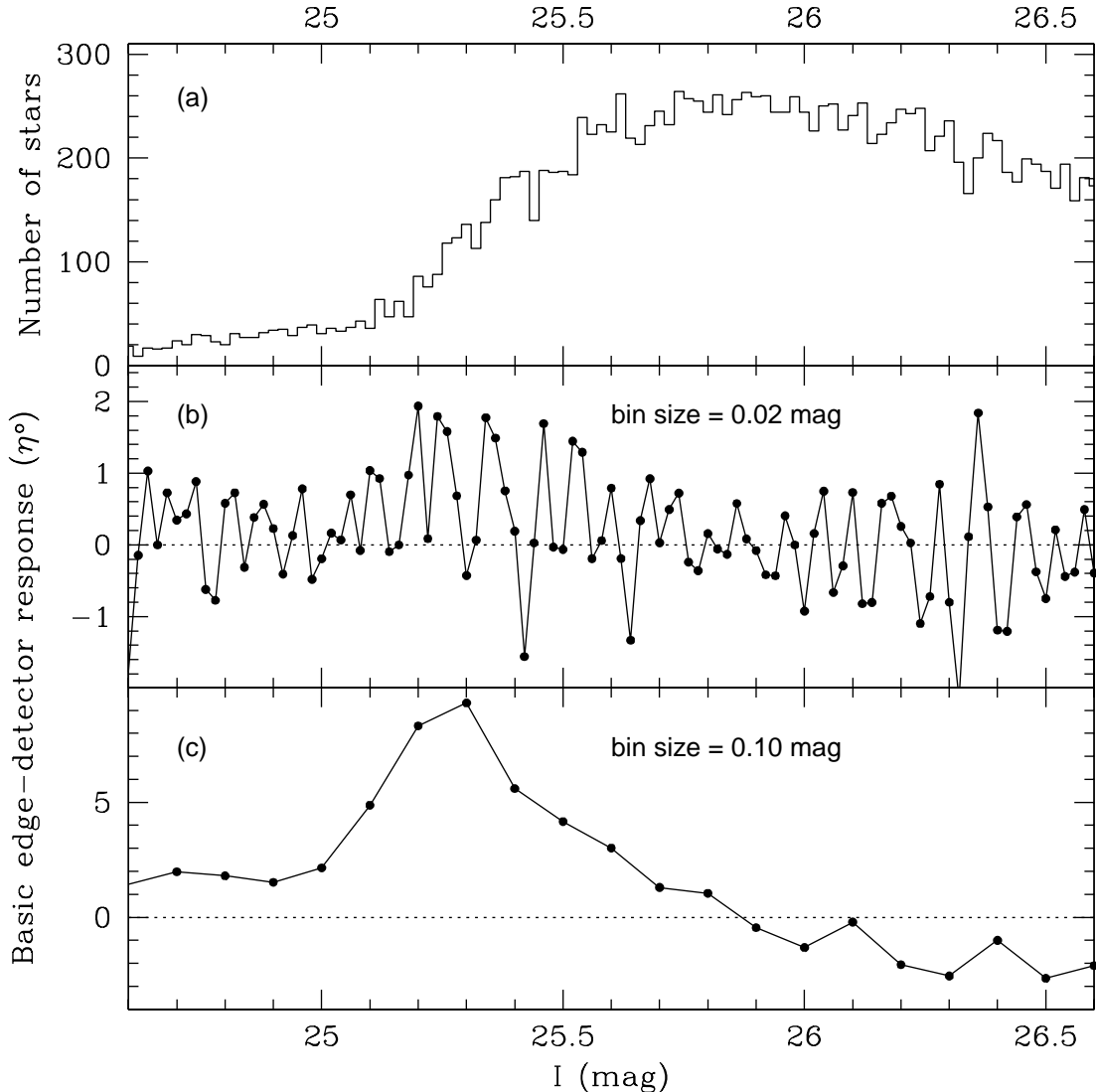


FIG. 4.— (a) Luminosity distribution of stars in the ACS images of NGC 4258 with colors corresponding to those of the TRGB ($1.6 < (V-I) < 3.0$). Bin sizes are 0.02 mag. (b) Basic edge-detector response, as defined by Eq. 4, for the histogram in (a). This detector response is highly dependent on noise-spikes within the luminosity profile, and may require a priori knowledge of the location of the TRGB to determine which peak corresponds to it. (c) Basic edge-detector response for a histogram with bin sizes of 0.10 mag bins. This detector response is more robust to noise, yielding a single unambiguous peak near the true location of the TRGB. However, it is not as precise as a filter applied to smaller magnitude bin sizes. We convolve the filter response in (b) and (c) into one robust, yet precise filter in Eq. 5 and Fig. 5.

Fig. 5 with a horizontal dashed line.

4.3. Error Analysis for the ACS data

We determined the statistical uncertainty on the I_{TRGB} measurement by applying our edge-detector algorithm to 63 sub-samples of stars, selected as a function of color, and with various sample sizes achieved by ranging the width of the selected color bins from 0.2 to 1.4 mag. Random variations in the result due to statistical fluctuations in the luminosity profile should be apparent from this test. We find a median value for I_{TRGB} of 25.24 mag within these sub-samples, which is the same as the result from the larger sample. There are variations in the solution among individual sub-samples, however, with the

largest variation seen in smaller color bin-size samples, which subsequently have smaller number statistics. Of the 63 sub-samples, 6 have I_{TRGB} measurements that are clear outliers, either around $I \sim 25.5$, or $I \sim 24.3$. These occur in relatively less populated bins, and are likely due to secondary peaks in the luminosity profile of these particular sub-samples being randomly higher than the peak at the location of the TRGB. In the case of data-sets with poor stellar number statistics, we therefore recommend applying a similar test in order to reject any outlying secondary solutions. Of the remaining 57 sub-samples, the individual measurements of I_{TRGB} vary by as much as ± 0.10 mag from the median in the 0.2 mag color bin size samples, ± 0.06 mag in the 0.3–0.4 mag bin size samples, and ± 0.04 mag in the 0.5–1.4 mag bin size

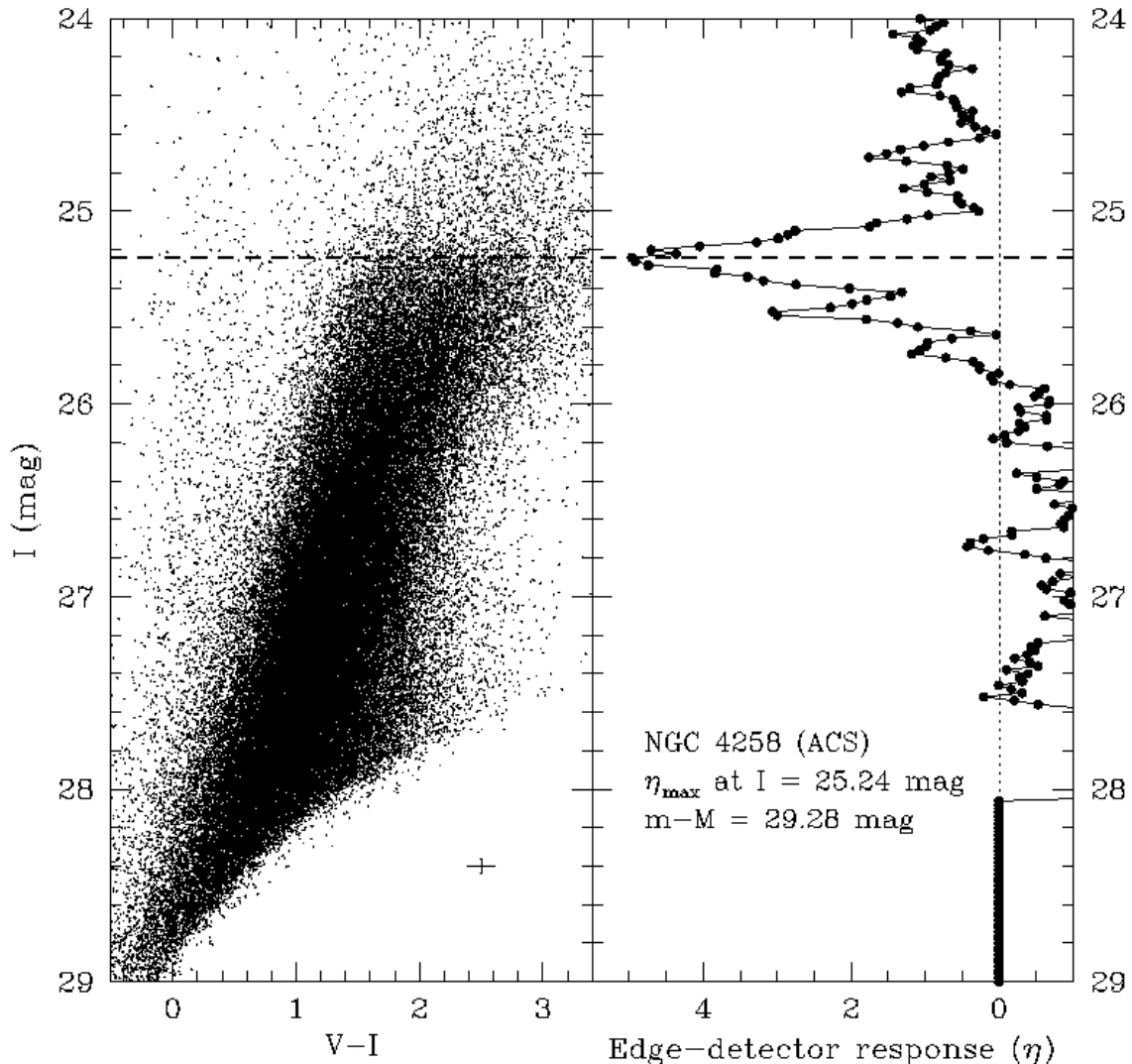


FIG. 5.— **Left:** The CMD from the NGC 4258 ACS data after applying the TRGB metallicity correction to each star (as derived from Eq.’s 2 and 3). **Right:** The value of the edge-detector response (η) from Eq. 5. The maximum peak of η gives our measured apparent magnitude of the TRGB, which is marked by the dashed horizontal line in both panels.

samples. For our measurement of I_{TRGB} from the largest sample ($1.6 < (V-I) < 3.0$), we adopt an uncertainty corresponding to the range of values achieved in the larger sub-samples, giving $I_{TRGB} = 25.24 \pm 0.04$ mag.

Systematic errors also contribute to the uncertainty of I_{TRGB} . One such possible error source is stellar crowding, which can lead to systematically brighter measurements for the TRGB (Madore & Freedman (1995)). To test the effects of crowding on our results, we applied our weighted edge detector to three separate sections of both chips in the ACS images, each with a different density of stars based on its proximity to the disk of the galaxy. The detected edge in each of these image sections varied within the statistical uncertainty of the detector (± 0.04 mag), and did not show any trend with increasing stellar density. Therefore, we conclude that crowding does not have a significant systematic effect in this ACS field.

4.4. Results from the WFPC2 Data

As a consistency check, we also applied our weighted edge-detector to the WFPC2 images of NGC 4258, providing a direct comparison of our measured TRGB apparent magnitude to that of Mouhcine et al. (2005) from the same data set. As evident in Fig. 1, the WFPC2 observations spatially overlap with the ACS observations, and thus sample largely the same population of halo stars. As can be seen in Fig. 2, however, there are far fewer stars detected in the WFPC2 images than the ACS images (mostly due to the superior sensitivity of the ACS detector). As such, the WFPC2 data will provide us with an indication of the applicability of our edge-detector to data with lower number statistics. Even so, the WFPC2 images still exceed the minimum requirements for a reliable measurement of the TRGB magnitude (Madore & Freedman 1995, Madore et al. 2008), with slightly less than 1000 stars in the 1 mag-width bin brighter than

the TRGB (even after the application of our color and χ value limits, as described below and in Section 3, respectively).

The metallicity-corrected CMD of the WFPC2 data is presented in the left panel of Fig. 6. As with the ACS data, we test the edge detector on 63 sub-samples of these stars as selected by color, and with various sample sizes within 0.2–1.4 mag bins in color. Because the WFPC2 data is shallower in V than the ACS data, we find that sub-samples including stars with $(V-I) \gtrsim 2.8$ mag lead to detected edges that are significantly fainter (by $\gtrsim 0.2$ mag) than the values obtained from bluer sub-samples of stars. As such, we apply slightly bluer color cuts to this data of $1.4 < (V-I) < 2.8$. The edge-detector response (η) from Eq. 5 for these data is shown in the right panel of Fig. 6. Although the detector response is noisier than that of the ACS data (see Fig. 5), the maximum peak is near the by-eye location of the TRGB, at $I_{TRGB} = 25.20 \pm 0.06$ mag, which is consistent with the median value of I_{TRGB} in the color-selected sub-samples. As with the ACS data, the uncertainty is obtained from the range of values of the detected edges in each of the sub-samples after rejecting extreme outliers. $I_{TRGB} = 25.20 \pm 0.06$ mag, as measured from the WFPC2 data, is 0.04 mag brighter than, but fully consistent with, $I_{TRGB} = 25.24 \pm 0.04$ mag, as measured from the ACS data. Madore & Freedman (1995) find that photometric errors and crowding can cause the discontinuity attributed to the TRGB to appear brighter than it really is. The WFPC2 data do have larger photometric errors than the ACS data, although crowding is not as much of an issue in the shallower WFPC2 images.

5. THE TRGB DISTANCE MODULUS; COMPARISON TO PREVIOUS RESULTS

As explained in Section 4.1, the absolute magnitude of our metallicity-corrected TRGB stars is taken to be $M_I^{TRGB} = -4.04 \pm 0.12$ mag. This leads to a distance modulus of $(m-M)_{ACS} = 29.28 \pm 0.04$ (random) ± 0.12 (systematic) mag, and $(m-M)_{WFPC2} = 29.24 \pm 0.06$ (random) ± 0.12 (systematic) mag. The ACS result is in exact agreement with the distance modulus of 29.28 ± 0.09 mag that was obtained through the Keplerian motion of nuclear water masers orbiting the central black hole (Herrnstein et al. 1999). The distance obtained through the orbital motions of these masers relies on simple, well-understood basic principles, and as such this distance determination for NGC 4258 carries high weight. Unfortunately, with only one example of this method to work with it is extremely hard to externally assess the systematics of this method. Hopefully more examples will be forthcoming.

As another consistency check, we compare our TRGB results to that of Mouhcine et al. (2005), who independently found the TRGB distance modulus from the same WFPC2 field we used for this analysis. Mouhcine et al. determined the apparent I-band magnitude of the TRGB by Gaussian-smoothing the luminosity function of all stars in the WFPC2 field with $(V-I) < 2$, and applying both a continuous function Sobel edge-detector, and maximum likelihood analysis. They then measured the average metallicity of their color-selected stars by fitting a Gaussian to the color distribution and apply-

ing the result to the metallicity-color relation from Lee et al. (1993). This average metallicity was then used in the distance modulus vs. I_{TRGB} equations in Lee et al. to find $(m-M)_\odot = 29.32 \pm 0.09$ (random) ± 0.15 (systematic) mag. This is 0.04 mag fainter than our result from the ACS data, and 0.08 mag fainter than our result from the WFPC2 data. However, despite different methods used in the edge-detector algorithm and treatment of the metallicity dependence of the TRGB magnitude, all of these results agree within the uncertainties. This apparent confirmation, on the other-hand, is not all that robust.

There is less agreement with Macri et al. (2006), who used their outer disk CMD data in an attempt to measure a TRGB distance. They noted a detection at $I = 24.42 \pm 0.02$ mag, which led them to a distance modulus of 29.41 ± 0.04 mag. Examination of their published CMD shows that they were working very close to their detection limit, and it is not clear how pure the Population II component would be in a region chosen for Population I Cepheid discovery. However, there is independent support for a large distance modulus.

Even more recently Rizzi et al. (2007) have published a pre-analysis of our data on NGC 4258 using their own TRGB detection methods and metallicity calibration. They claim a tip detection at 25.49 ± 0.05 mag, corresponding to a metallicity-corrected distance modulus of 29.42 ± 0.06 mag. These moduli respectively are 7 and 3 sigma away from our value. Rizzi et al. (2007) note that their value puts them in very good agreement with the Macri et al. (2006) Cepheid distance modulus, but it places them 2-sigma away from the maser distance. To address this discrepancy, Macri et al. re-calculated their TRGB tip magnitude using the same metallicity correction, color limits, and reddening correction that were applied in this paper (Tully, B., private communication). They found a revised I-band tip magnitude of 25.26 mag, which is in excellent agreement with our value of 25.24 ± 0.04 mag. They also find a difference of 0.09 mag in the results of their own analysis when adjusting for metallicity before vs. after running their tip finder. This indicates that the 0.14 mag difference between the published Rizzi et al. (2007) distance modulus and our own is likely not due to the tip detection method itself, but to systematic differences in the application of the metallicity correction. This results in a systematic uncertainty associated with the calibration zero point, which is encompassed by our quoted systematic uncertainty of ± 0.12 mag.

Prompted by these differences, we now take an independent look at the Cepheid data.

6. THE CEPHEID DATA FOR NGC 4258

Macri et. al (2006) present VI data for 281 Cepheids in two radially separated fields in the disk of NGC 4258. From these data they derive a distance-modulus difference of 10.88 ± 0.04 mag between NGC 4258 and the LMC. Scaled to the value of the LMC distance modulus (18.50 mag) adopted by the HST Key Project (Freedman et al. 2001) this corresponds to a distance modulus of 29.38 mag for NGC 4258. How robust is this number?

So as to be totally consistent with the Key Project zero

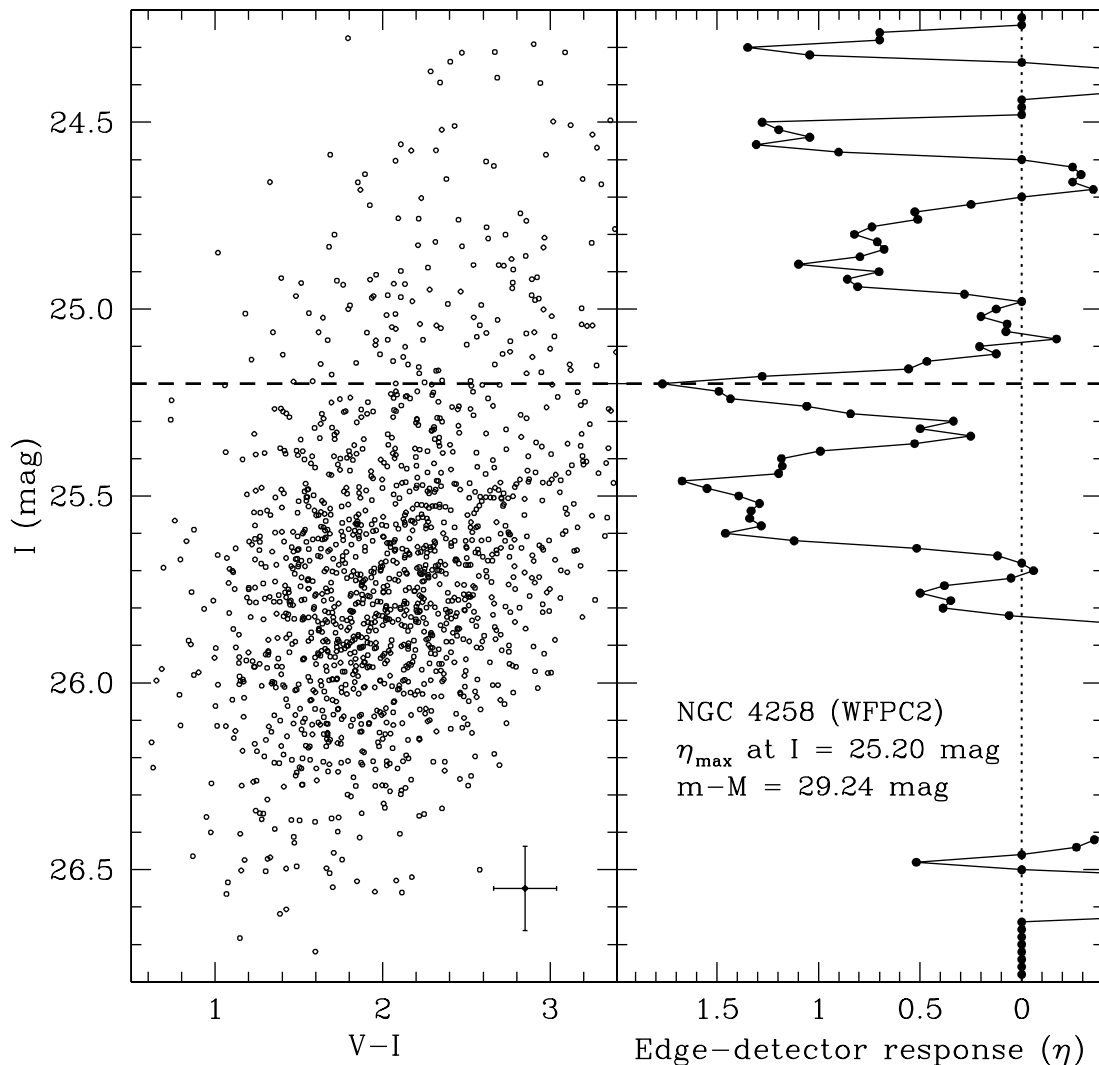


FIG. 6.— **Left:** The CMD from the NGC 4258 WFPC2 data after applying the TRGB metallicity correction to each star (as derived from Eq.’s 2 and 3). **Right:** The value of the edge-detector response (η) from Eq. 5. The maximum peak of η gives our measured apparent magnitude of the TRGB, which is marked by the dashed horizontal line in both panels. This agrees with the result from the ACS data within the uncertainties.

points and methodology we restrict ourselves to Cepheids in NGC 4258 that have periods in excess of 10 days. This has the added advantage of using stars with the highest signal to noise, and implicitly avoiding other issues concerning the putative change in slope of the PL (period-luminosity) relation below 10 days, and the possible contamination of the data set by over-tone pulsators that are also only found below 10 days in period.

Using those restricted samples of Cepheids in each of the two radial fields, and the method described in Freedman et al. (1994), we find the following:

Outer Field: $\mu_V = 29.80 \pm 0.10$, $\mu_I = 29.66 \pm 0.06$

Inner Field: $\mu_V = 29.84 \pm 0.04$, $\mu_I = 29.60 \pm 0.03$

The very first thing to notice is that the apparent moduli for these two distinct fields in both bands are statistically the same to within one sigma of each other. However, there are slight differences, and these in turn

give rise to systematic differences in the formally derived reddenings for each of the two fields: the Inner Field Cepheids have a mean reddening of $E(V - I) = 0.24$ mag while the Outer Field Cepheids have a calculated mean reddening of $E(V - I) = 0.14$ mag. These differences in reddening get further multiplied up (by the ratio of total-to-selective absorption) yielding systematic differences in the extinction: $A_V(\text{inner}) = 0.58$ mag and $A_V(\text{outer}) = 0.34$ mag. Ultimately the two extinction-corrected (true) moduli become:

Outer: $\mu_o = 29.45 \pm 0.08$

Inner: $\mu_o = 29.26 \pm 0.03$

This difference represents a 2-sigma significance of separation amounting to about 0.2 mag. The presumptive interpretation is that this difference is due to metallicity differences between the inner and outer field Cepheids. There are, however, other possible interpretations of the

NGC 4258

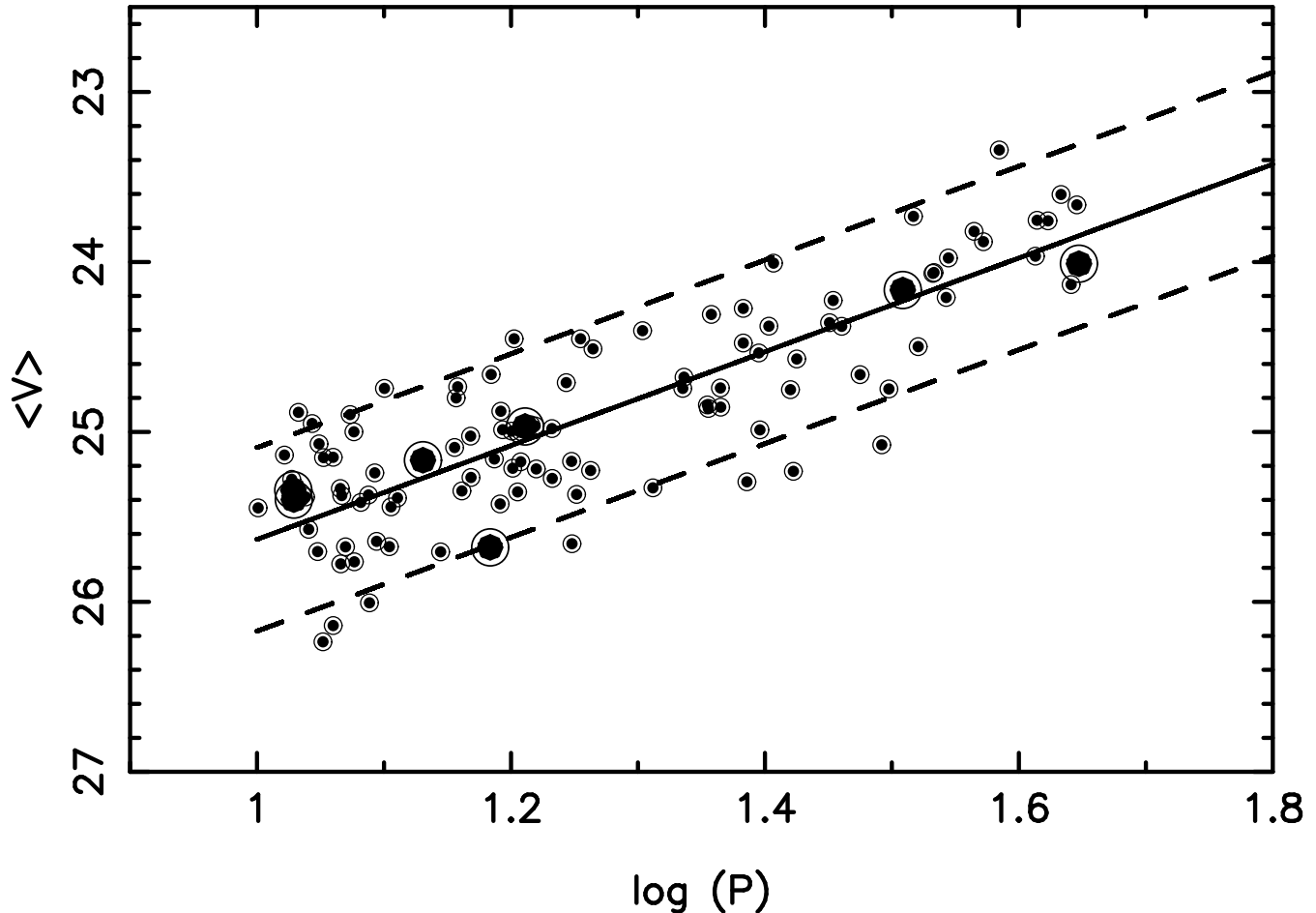


FIG. 7.— The V-band PL relation for all long-period ($P > 10$ d) Cepheids in NGC 4258 using data from Macri et al. (2006). Small symbols are for Cepheids in the inner field; large symbols track the Cepheids in the outer field. The solid line represents the expected trend from calibrations, with the dotted lines marking the $2\text{-}\sigma$ variation from this trend (Madore & Freedman 1991). Note the significantly smaller scatter of the larger symbols with respect to the expected range.

data. The first is that the reddening law may be different between the two fields. The second is that small number statistics have generated the difference. That is, for the small sample of stars in the outer field we just got (un)lucky. We offer up evidence in support of that possibility below.

First we set aside the possibility of systematically changing the reddening law for a different paper. The implications of changing the reddening law from galaxy to galaxy, or from place to place within a given galaxy are too far-reaching for us to give it the necessary attention in this paper. Suffice it to say that if the canonical value of $R_{VI} \simeq 2.4$ is adopted for the inner field, the two moduli can be made to agree if $R_{VI} \simeq 4.0$ in the outer field. The second possibility is easy to consider, and it has few consequences beyond this particular application. It is also motivated by our earlier observation that the apparent moduli in the two fields were statistically identical but systematically diverged as reddening corrections were derived and applied.

To shed some light on the possibility that there may

be no real differences in the two Cepheid populations, we now merge the two data sets and invite the reader to inspect and consider the results. In Figures 7 and 8 we show the apparent V and I-band PL relations for the Cepheids in NGC 4258; the large filled circles are the Cepheids in the outer field, and the more abundant smaller filled circles are Cepheids in the inner field. Had there been no differences in the symbols the inner and outer-field Cepheids would be inseparable. That is, the outer-field Cepheids would fall entirely within the known bounds of the fiducial PL relation instability strip; but they do not fill the strip. This latter point is important. Because the outer Cepheids do not fully sample the strip, their mean is suspect and may well be biased. The width of the instability strip that these particular Cepheids delineate is, in fact, about a factor of two smaller than the known width, whether that is measured in the I-band, the V-band or, more importantly, in the reddening-free W-PL relation (Madore 1982). The latter relation is shown in Figure 9, where the outer-field Cepheid data points are so tightly co-linear that they have a measured

NGC 4258

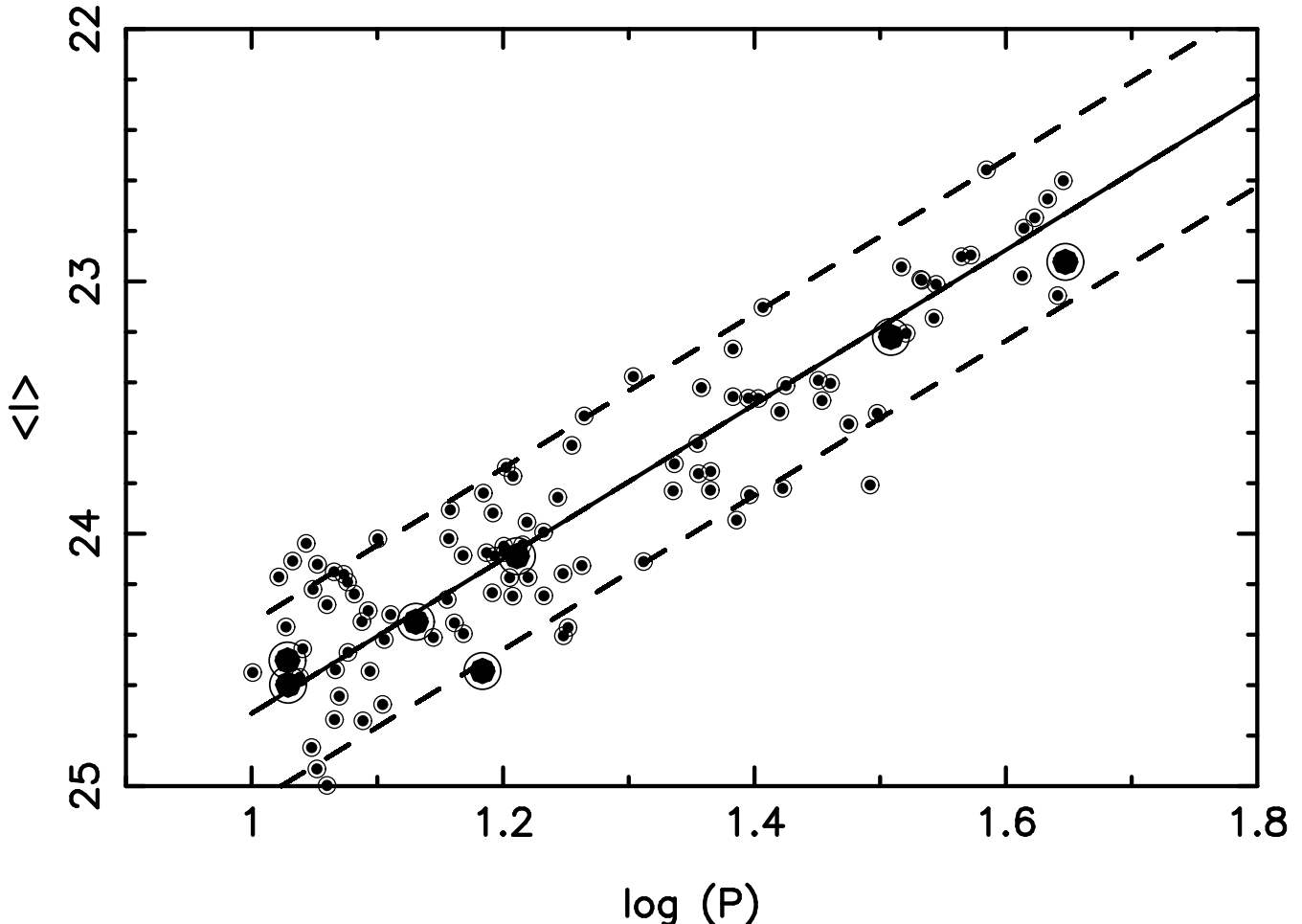


FIG. 8.— The I-band PL relation for all long-period Cepheids in NGC 4258 using data taken from Macri et al. (2006). Small symbols are for Cepheids in the inner field; large symbols track the Cepheids in the outer field. The solid line represents the expected trend from calibrations, with the dotted lines marking the $2\text{-}\sigma$ variation from this trend (Madore & Freedman 1991). Note the significantly smaller scatter of the larger symbols with respect to the expected range.

width that is about a factor of four smaller than the intrinsic width.

We conclude that the outer-field Cepheids are likely to be a biased sub-set of Cepheids, in that they fail the minimalist requirement of sampling the entire width of the instability strip before they can be considered to be a fair sample for either absolute or comparative purposes.

Using the combined data set of 113 long-period Cepheids, irrespective of their position in the galaxy, we derive the following apparent moduli:

$$\mu_V = 29.79 \pm 0.03, \mu_I = 29.58 \pm 0.02$$

With a derived mean reddening of $E(V - I) = 0.21 \pm 0.02$ mag, this leads to a true distance modulus of

$$\mu_o = 29.28 \pm 0.02$$

This is the true distance modulus to NGC 4258 (corresponding to a metric distance of 11.4 Mpc) that we believe best reflects the critically combined Cepheid data. It also coincidentally agrees remarkably well, indeed exactly, with the independently determined maser distance modulus of 29.28 ± 0.09 mag. Moreover it also agrees

with our TRGB distance modulus of 29.28 ± 0.04 mag.

Knowing the improbability of these alignments, and given the importance of these comparisons combined with the published divergence of solutions, this is probably not to be the last word on the subject. However, it is an interesting convergence of three important distance measurements to a critically important galaxy.

These results show that the TRGB determination method described here is reasonably accurate in determining the distance to this single galaxy. We have also found it to be applicable to several other, more distant and fainter galaxies, which we will address in the subsequent papers of this series.

This research has made use of the NASA/IPAC Extragalactic Database (NED) which is operated by the Jet Propulsion Laboratory, California Institute of Technology, under contract with the National Aeronautics and Space Administration; and also made use of NASA's Astrophysics Data System. We thank the referee, Brent

NGC 4258

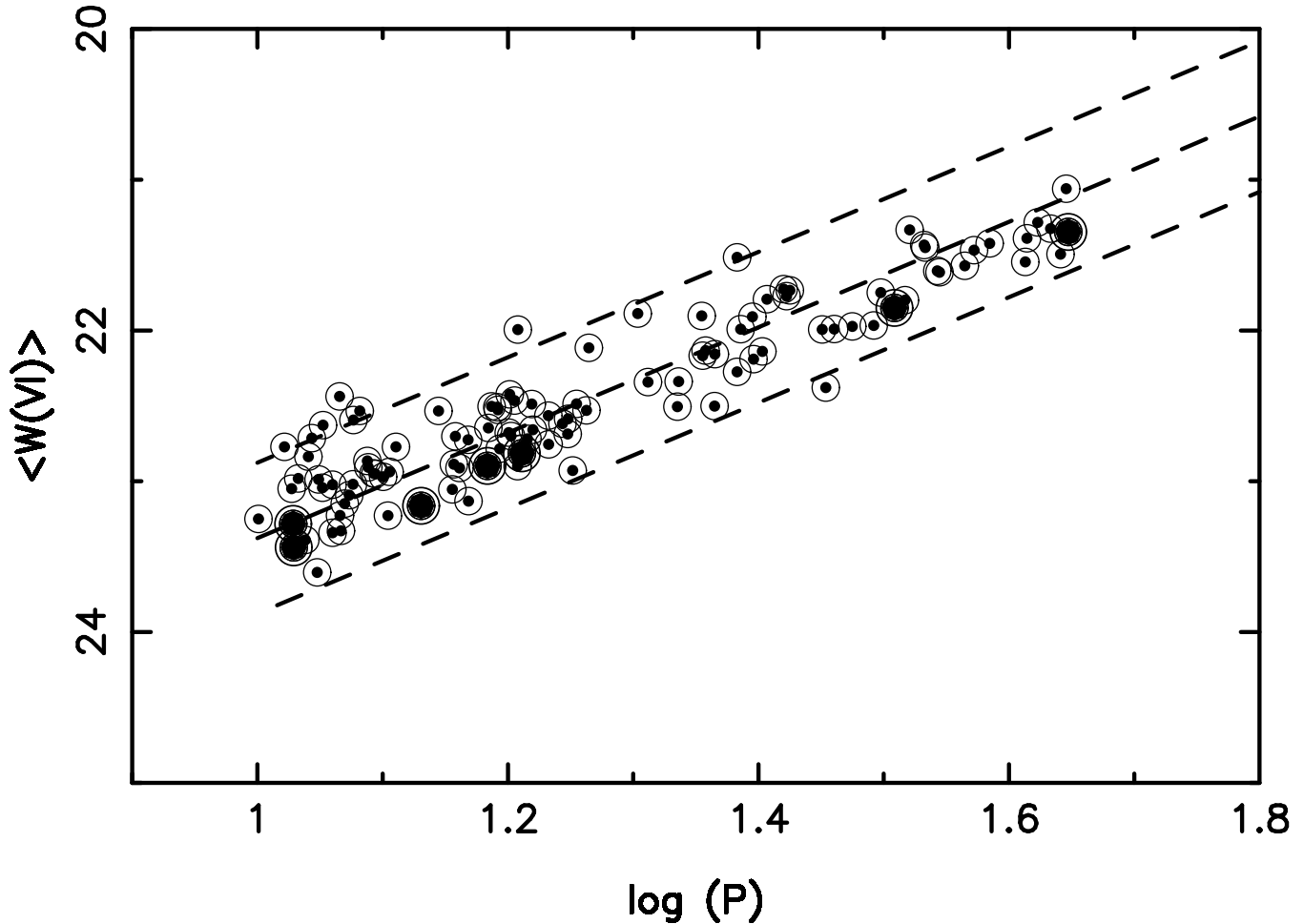


FIG. 9.— The reddening-free W PL relation for all long-period Cepheids in NGC 4258 using data taken from Macri et al. (2006). As in the previous two figures the small symbols are for Cepheids in the inner field. Large symbols track the Cepheids in the outer field. The solid line represents the expected trend from calibrations, with the dotted lines marking the 2σ variation from this trend (Madore & Freedman 1991). Once again, there is significantly smaller scatter (this time by nearly a factor of four) of the larger symbols with respect to the expected range. In this case none of the scatter can be due to differential reddening.

Tully, for his constructive comments.

REFERENCES

- Bellazzini, M., Ferraro, F. R., & Pancino, E. 2001, *ApJ*, 556, 635
 Bellazzini, M., Ferraro, F. R., Sollima, A., Pancino, E., & Origlia, L. 2004, *A&A*, 424, 199
 Cioni, M. R. L., van der Marel, R.P., Loup, C., & Habing, H. J. 2000, *A&A*, 359, 601
 Dolphin, A. E. 2000, *PASP*, 112, 1397
 Frayn, C. M., & Gilmore, G. F. 2003, *MNRAS*, 339, 887
 Freedman, W. L., et al. 1994, *ApJ*, 427, 628
 Freedman, W. L., et al. 2001, *ApJ*, 553, 47
 Herrnstein, J. R., et al. 1999, *Nature*, 400, 539
 Iben, I., & Renzini, A. 1983, *ARA&A*, 21, 271
 Lee, M. G., Freedman, W. L., & Madore, B. F. 1993, *ApJ*, 417, 553
 Macri, L. M., Stanek, K.Z., Bersier, D., Greenhill, L.J., & Reid, M.J. 2006, *ApJ*, 652, 1133
 Madore, B. F. 1982, *ApJ*, 253, 575
 Madore, B. F. & Freedman, W. L. 1991, *PASP*, 103, 933
 Madore, B. F., & Freedman, W. L. 1995, *AJ*, 109, 1645
 Madore, B. F., Mager, V., & Freedman, W.L. 2008, *ApJ*, submitted
 Makarov, D., Makarova, L., Rizzi, L., Tully, R. B., Dolphin, A. E., Sakai, S., Shaya, E. J. 2006, *AJ*, 132, 2729
 McConnachie, A. W., Irwin, M. J., Ferguson, A. M. N., Ibata, R. A., Lewis, G. F., & Tanvir, N. 2004, *MNRAS*, 350, 243
 Méndez, B., Davis, M., Moustakas, J., Newman, J., Madore, B. F., & Freedman, W. L. 2002, *AJ*, 124, 213
 Mouhcine, M., Ferguson, H. C., Rich, R. M., Brown, T. M., & Smith, T. E. 2005, 633, 810
 Renzini, A. 1991, in *Observational Tests for Cosmological Inflation*, ed. T. Shanks, A. J. Banday, R. S. Ellis, C. S. Frenk, & A. W. Wolfendale (Boston: Kluwer), 131
 Rizzi, L., Tully, R. B., Makarov, D., Makarova, L., Dolphin, A. E., Sakai, S., Shaya, E. J. 2007, *ApJ*, 661, 815
 Sakai, S., Madore, B. F., & Freedman, W. L. 1996, 461, 713
 Salaris, M., & Cassisi, S. 1998, *MNRAS*, 298, 166
 Sarajedini, A., et al. 2002, *ApJ*, 567, 915
 Sirianni, M., et al. 2005, *PASP*, 117, 1049
 Stetson, P. B. 1987, *PASP*, 99, 191
 Stetson, P. B. 1994, *PASP*, 106, 250